AUTOPHAGY
2021, VOL. 17, NO. 6, 1393–1409
https://doi.org/10.1080/15548627.2020.1761742

Taylor & Francis
Taylor & Francis Group

RESEARCH PAPER

Involvement of CASP9 (caspase 9) in IGF2R/CI-MPR endosomal transport

Jie Han[a], Leslie A. Goldstein[a], Wen Hou[a], Simon C. Watkins[b], and Hannah Rabinowich[a]

[a]Departments of Pathology, University of Pittsburgh School of Medicine and the University of Pittsburgh Cancer Institute, Pittsburgh, PA, USA; [b]Cell Biology, University of Pittsburgh School of Medicine and the University of Pittsburgh Cancer Institute, Pittsburgh, PA, USA

ABSTRACT

Recently, we reported that increased expression of CASP9 pro-domain, at the endosomal membrane in response to HSP90 inhibition, mediates a cell-protective effect that does not involve CASP9 apoptotic activity. We report here that a non-apoptotic activity of endosomal membrane CASP9 facilitates the retrograde transport of IGF2R/CI-MPR from the endosomes to the trans-Golgi network, indicating the involvement of CASP9 in endosomal sorting and lysosomal biogenesis. CASP9-deficient cells demonstrate the missorting of CTSD (cathepsin D) and other acid hydrolases, accumulation of late endosomes, and reduced degradation of bafilomycin A_1-sensitive proteins. In the absence of CASP9, IGF2R undergoes significant degradation, and its rescue is achieved by the re-expression of a non-catalytic *CASP9* mutant. This endosomal activity of CASP9 is potentially mediated by herein newly identified interactions of CASP9 with the components of the endosomal membrane transport complexes. These endosomal complexes include the retromer VPS35 and the SNX dimers, SNX1-SNX5 and SNX2-SNX6, which are involved in the IGF2R retrieval mechanism. Additionally, CASP9 interacts with HGS/HRS/ESCRT-0 and the CLTC (clathrin heavy chain) that participate in the initiation of the endosomal ESCRT degradation pathway. We propose that endosomal CASP9 inhibits the endosomal membrane degradative subdomain(s) from initiating the ESCRT-mediated degradation of IGF2R, allowing its retrieval to transport-designated endosomal membrane subdomain(s). These findings are the first to identify a cell survival, non-apoptotic function for CASP9 at the endosomal membrane, a site distinctly removed from the cytoplasmic apoptosome. Via its non-apoptotic endosomal function, CASP9 impacts the retrograde transport of IGF2R and, consequently, lysosomal biogenesis.

Abbreviations: ACTB: actin beta; ATG7: autophagy related 7; BafA1: bafilomycin A_1; CASP: caspase; CLTC/CHC: clathrin, heavy chain; CTSD: cathepsin D; ESCRT: endosomal sorting complexes required for transport; HEXB: hexosaminidase subunit beta; HGS/HRS/ESCRT-0: hepatocyte growth factor-regulated tyrosine kinase substrate; IGF2R/CI-MPR: insulin like growth factor 2 receptor; ILV: intraluminal vesicles; KD: knockdown; KO: knockout; M6PR/CD-MPR: mannose-6-phosphate receptor, cation dependent; MEF: murine embryonic fibroblasts; MWU: Mann-Whitney U test; PepA: pepstatin A; RAB7A: RAB7, member RAS oncogene family; SNX-BAR: sorting nexin dimers with a Bin/Amphiphysin/Rvs (BAR) domain each; TGN: trans-Golgi network; TUBB: tubulin beta; VPS26: VPS26 retromer complex component; VPS29: VPS29 retromer complex component; VPS35: VPS35 retromer complex component.

ARTICLE HISTORY
Received 6 May 2019
Revised 20 April 2020
Accepted 23 April 2020

KEYWORDS
Caspase-9; endosome; HGS/HRS/ESCRT-0; IGF2R/CI-MPR; lysosome; retromer

Introduction

Our recent studies have identified non-apoptotic activities for CASP9, including its involvement in the initial phase of autophagosome formation [1], and in a cell-protective endosomal membrane function that has not yet been molecularly elucidated [2]. Our studies suggest that CASP9 interaction with ATG7 is one of the mechanisms by which CASP9 contributes to the early phase of autophagy. The ATG7-CASP9 interaction serves to inhibit CASP9 apoptotic activity and enhance autophagosome formation [1]. Recently, a new study has confirmed the involvement of CASP9 in autophagosome formation [3]. Also, we previously reported the upregulated expression of CASP9 pro-domain at the endosomal membrane in response to HSP90 inhibition, where CASP9 mediates a non-apoptotic cell survival function [2] that has been investigated in the current study. Although the critical function of caspases in apoptosis is firmly established, it has become evident that certain caspases mediate other cellular processes distinct from apoptotic cell death that often still require their catalytic activity [4,5]. Thus, two previous studies identified non-apoptotic activities for CASP9 that are dependent on its catalytic activity, including myotube formation in the skeletal muscle [6] and the involvement of CASP9 enzymatic activity in lysosomal function [7]. However, CASP9 interaction with ATG7 and its impact on the autophagosome formation process are independent of its caspase catalytic activity [1]. In the current study, we report a new non-apoptotic function for CASP9 that occurs on the endosomal membrane impacting lysosome biogenesis, and by extension, the late phase of autophagy.

CONTACT Hannah Rabinowich, rabinow@pitt.edu The Hillman Cancer Center, University of Pittsburgh Cancer Institute, Research Pavilion Rm. G17c, 5117 Centre Avenue, Pittsburgh, PA 15213, USA

Supplemental data for this article can be accessed here.

Lysosomes are membranous organelles that contain more than 50 acid hydrolases that function in the degradation of proteins and organelles delivered by the autophagic, phagocytic, and endocytic pathways. As assessed by electron microscopy, lysosomes are heterogeneous in size and morphology, often with electron-dense content, and sometimes with multilamellar membrane whorls [8,9]. Achieving a full understanding of lysosomal biogenesis remains challenging, particularly with regard to the molecular distinction between the various phases of late endosomes, endolysosomes, and reformed lysosomes [9]. Importantly, all known lysosomal markers, including LAMP2, are shared by the various precursor membranous organelles that participate in the transport to and fusion with the lysosomes [10,11]. However, lysosomes are distinguished from late endosomes and other intermediaries by the absence of mannose-6-phosphate receptors (MPRs) [9]. Two types of MPRs, cation-dependent (M6PR) and cation-independent (IGF2R), are involved in the major pathway of delivering newly synthesized acid hydrolases to the lysosomes via endosomes [12]. In particular, acid hydrolases that are tagged with an endosomal-targeting mannose 6-phosphate sugar bind to one of the two MPR types in the trans-Golgi network (TGN) and traffic via clathrin-coated vesicles to the endosomes. Due to the low pH in the early/late endosomes, the MPR-ligand complexes dissociate, and the MPRs recycle back to the TGN for further rounds of transport [13]. The retrieval of unoccupied MPRs to the TGN involves a retrograde route that is mediated by the endosomal membrane transport protein complexes that include the retromer, SNX dimers, and destination/cargo-specific sorting nexins (SNX) [14–16]. The mammalian retromer is a heterotrimer of VPS26A/B-VPS35-VPS29, where VPS35 is the major cargo interacting protein [15]. The nexin dimers (SNX-BAR) include the SNX1-SNX5 and SNX2-SNX6 complexes, where each of the dimer components contains 2 membrane-binding domains, including a BAR domain and a phosphoinositide-binding PX domain [14]. The retromer trimer is recruited to the endosomal membrane by interactions with both the GTP-bound form of the RAB7A GTPase and SNX3 [15,17,18]. The SNX dimers and SNX3 are recruited to the endosomal membrane through binding between their PX domains and phosphatidylinositol-3 phosphate (PtdIns3P) in the membrane [15]. PtdIns3P is generated by the Class III PtdIns 3-kinase (PtdIns3K), which is an indirect interactor with RAB7A-GTP and is dependent on RAB7A's nucleotide cycling activity for its kinase activity [19]. The nexin dimers assemble to promote the formation of endosomal membrane tubules into which cargo proteins are delivered [15]. Accumulating evidence suggests that clathrin, whose involvement in the anterograde transport from the TGN to the endosomes via clathrin-coated vesicles is well established, also has an indirect role in retromer biology [20–24]. In contrast to the yeast retromer, where the retromer trimer interacts with the nexin dimers, each of these complexes appears to have its own transport capacity in mammals [25,26]. Multiple previous studies have documented the involvement of the retromer trimer in the IGF2R retrieval mechanism [27–32]. However, this issue has become controversial, as recent studies that utilized CRISPR-Cas9 KO of *VPS35, SNX1/2*, or *SNX5/6* have determined the involvement of the SNX-BAR dimers, and not VPS35, in the retrograde transport of IGF2R [25,26,33,34]. Confoundingly, another recent study has determined a selective involvement of the retromer in the retrograde sorting of IGF2R, which depends on specific TGN-located tethering proteins that capture the IGF2R-retromer complex [35].

In the current study, we obtained evidence that CASP9 is an effector of endosome-lysosome dynamics. Our findings suggest that CASP9 endosomal function involves the retrieval of unoccupied IGF2Rs from late endosomes into their retrograde route in a manner that is not dependent on CASP9's caspase catalytic activity. As deduced from newly identified complexes of CASP9 with endosomal membrane transport proteins, as well as with the endosomal degradative machinery, we propose that CASP9 participates in a crosstalk mechanism between the endosomal subdomains that selects between retrieval and degradation outcomes for the endosomal IGF2R.

Results

Involvement of CASP9 in endosomal maturation

In our efforts to elucidate the autophagic function of CASP9, we observed that its knockdown (KD) impacts the cellular localization of LAMP2-positive vesicles in a manner similar to that of the treatment using saturating doses of the cathepsin inhibitors E64D and pepstatin A (E/P, Figure 1A,B). Thus, in CASP9-deficient cells, LAMP2-positive vesicles changed their cytoplasmic distribution to a substantial accumulation at a juxtanuclear area. The juxtanuclear accumulation of LAMP2-positive vesicles was confirmed with 3 distinct LAMP2-specific Abs, following *CASP9* KD, but not *CASP8* KD (**Fig. S1 and S2**). Co-treatment by *CASP9* siRNA and saturating doses of E/P demonstrated an additive effect of such juxtanuclear accumulation of LAMP2-positive vesicles, potentially suggesting the concurrent inhibition of both lysosomes and pre-lysosomal vesicles that express LAMP2. This change in LAMP2 vesicle dispersion was not associated with an increase in the LAMP2 cellular level (Figure 1C), suggesting lysosomal inhibition and/or a maturation arrest of LAMP2-positive vesicles. Of note, LAMP2 is expressed on both the late endosomes and lysosomes [11], and blockage of either of these maturation/activity phases is expected to impact the cell's overall lysosomal activity.

To start characterizing a potential endosomal maturation block, we tested the impacts of CASP9 deficiency on lysosomal function [36,37]. To distinguish the cellular lysosomal function from a concomitant proteasomal activity, we assessed the significance of CASP9 expression for the degradation of ubiquitinated proteins in the presence of the proteasome inhibitor, MG132. A concurrent proteasomal inhibition was required to block a compensatory proteasomal activity, which is usually upregulated upon lysosomal inhibition [38–41]. While no difference was detected in 2% SDS-soluble ubiquitinated proteins obtained from WT vs. *casp9* KO MEF (**Fig. S3**), *casp9* KO MEF exhibited an increased level of SDS-insoluble ubiquitinated proteins (Figure 1D-L), as determined by the filter-trap assay [42–44]. The SDS-insoluble proteins

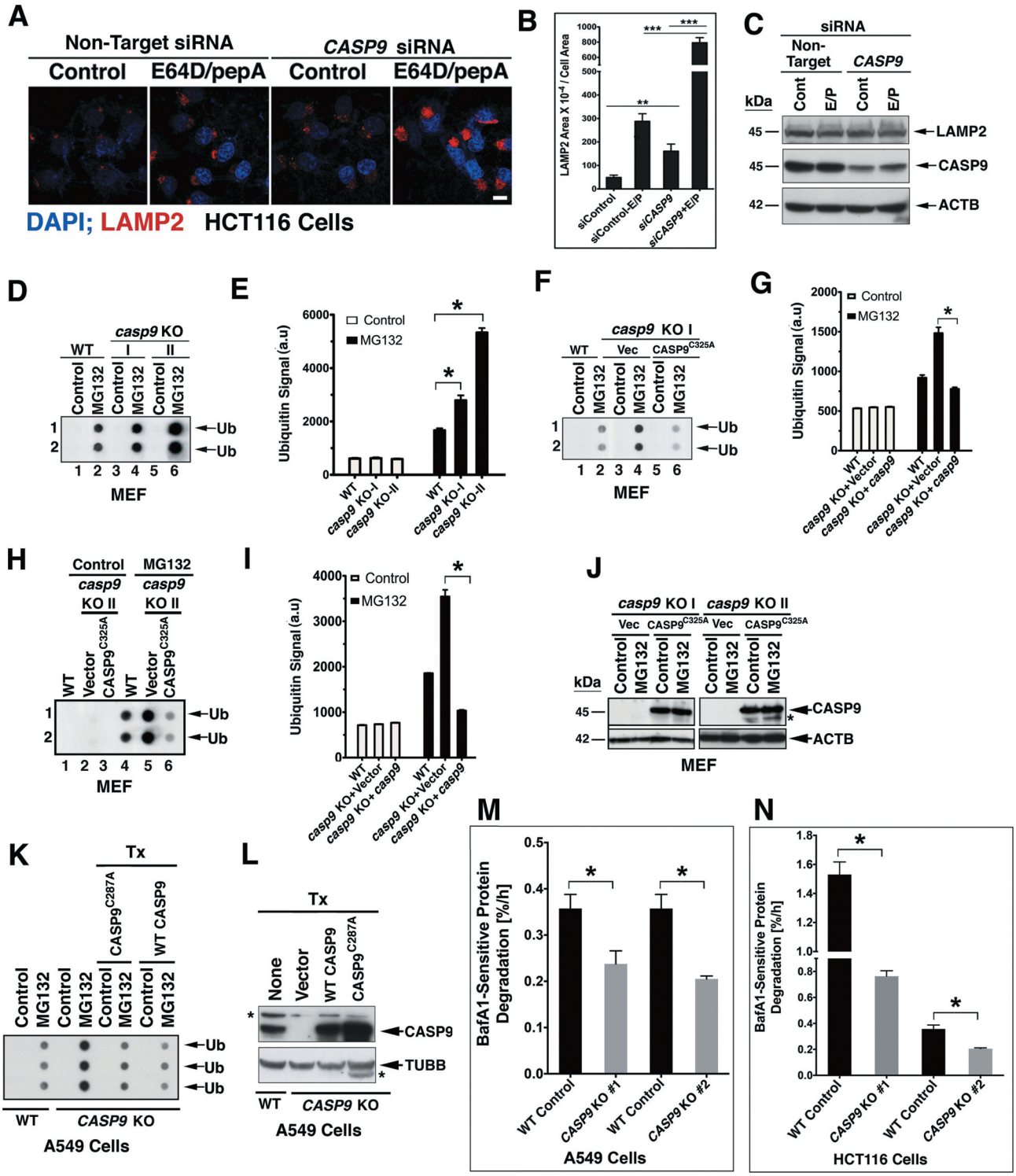

Figure 1. CASP9 is involved in lysosome cellular localization and activity. (A) *CASP9* KD alters the distribution of LAMP2 in an additive manner to that of cathepsin inhibitors. HCT116 cells were treated with *CASP9* siRNA or non-target siRNA in the presence of E64D/pepA (10 μM each) or vehicle control. The cells were assessed by a confocal microscope for LAMP2 (mouse Ab sc-18822) and DAPI staining. Scale bar: 40 μm. (B) LAMP2 quantification. The data are means±SEM of approximately 50 cells per treatment in at least 3 independent experiments. *** = $p < 0.0001$; ** = $p < 0.001$ (MWU). Staining with additional anti-LAMP2 Abs are shown in **Fig. S1 and S2**. (C) Immunoblotting of lysates of the cells used in A. (D-L) CASP9 impacts lysosomal efficiency in the clearance of SDS-insoluble ubiquitinated proteins in *casp9* KO MEF and *CASP9* KO tumor cells. (D-E) *casp9* KO MEF (clones I and II) exhibit decreased lysosomal clearance of ubiquitinated aggregates as compared to WT MEF. WT and *casp9* KO MEFs were treated with MG132 (1 μM) and the resulting SDS-insoluble ubiquitinated aggregates were detected by the filter-trap assay. Duplicate spots are shown for each treatment. (E) Densitometric quantification of the immunoblotted SDS-insoluble fractions shown in D. The data are means±SEM of four replicates in each of three independent experiments with similar results. The asterisks indicate statistical significance at $p < 0.05$ (MWU). (F-I) The defect in aggregate protein clearance in *casp9* KO MEF is reversed by the transfection with a plasmid encoding the murine non-catalytic CASP9^{C325A} mutant. Quantification of the results shown in F and H are presented in G and I, respectively, and are means±SEM as described in E. (J) Expression levels of CASP9 in the cells utilized in F and H. (K) The reduced lysosomal clearance of ubiquitinated aggregates in CRISPR-Cas9 *CASP9* KO A549 cells is rescued by the transfection of plasmids encoding either WT CASP9 or non-catalytic CASP9^{C287A} mutant. (L) Expression of CASP9 in one of the A549 cell preparations used in K. (M-N) BafA1-sensitive degradation in parental/WT controls and CRISPR-Cas9 *CASP9* KO clonal cell lines, including A549 (M) and HCT116 (N). #1 and #2 indicate independent experiments performed with different CRISPR-CAS9 *CASP9* KO clones for each of the cell lines. The data are means±SEM of 6 replicates in at least 2 independent experiments. *$p < 0.05$ (MWU).

were only detected in the presence of MG132, suggesting that the impairment in lysosomal degradation mediated by CASP9 deficiency is indeed compensated for by the proteasomal activity. Transfection of a catalytically inactive murine CASP9^{C325A} mutant markedly reduced the levels of these SDS-insoluble proteins. These findings were confirmed both in *casp9* KO MEF transfected with murine non-catalytic CASP9^{C325A} mutant (Figure 1D-J) and in a human CRISPR-Cas9 *CASP9* KO A549 NSCLC clonal cell line transfected with either human CASP9 WT or non-catalytic CASP9^{C287A} mutant (Figure 1K,L). As the experiments were performed in the presence of proteasomal inhibition, these findings suggest the involvement of CASP9 in the lysosomal degradation of ubiquitinated proteins.

We further compared the BafA1-sensitive lysosomal degradative activity of the parental (WT control) and CRISPR-Cas9 *CASP9* KO clones from 2 tumor cell lines (Figure 1M,N). A significantly reduced degradation of BafA1-sensitive proteins was detected in all tested *CASP9* KO clones as compared to their WT controls. These findings suggest that CASP9 deficiency compromises certain lysosomal activities, but they neither indicated the exact cellular site nor the specific molecular activity involved.

Using transmission electron microscopy, we observed in *casp9* KO MEF an accumulation of the late endosomes with apparent undegraded cargoes, whose per cell number was significantly reduced by stable expression of the non-catalytic CASP9^{C325A} mutant (Figure 2A,B**, and S4**).

To further characterize the impact of CASP9 on the potential accumulation of late endosomes, we assessed for the presence of RAB7A-positive vesicles in WT vs. *casp9* KO MEF. We observed a significant increase in the accumulation pattern of RAB7A in *casp9* KO MEF as compared to WT MEF, and this difference was accentuated in the presence of MG132 that blocks the proteasomal contribution to the degradation process (Figure 2C,D). Transfection of the plasmid encoding the CASP9^{C325A} mutant into *casp9* KO MEF reduced the presence of RAB7A-expressing late endosomes. Also, the observed changes in the area occupancy of RAB7A were not associated with an increase in its cellular expression level, as determined by immunoblotting (Figure 2E). These findings suggest that CASP9 has a non-apoptotic function that impacts the cellular distribution of RAB7A.

Association of CASP9 with endosomal membrane complexes

Since CASP9 is known to function in the cytoplasm as a component of the apoptosome, its non-apoptotic impact on the endo-lysosomal degradation activity indicates that there is a distinct subcellular localization where it is sequestered from either the cytoplasm or mitochondria [45]. As CASP9 impacts the cellular distribution of RAB7A, we tested for their potential cellular association. Indeed, when co-expressed in *casp9* KO MEF, DsRed-CASP9^{C325A} and GFP-RAB7A demonstrated a distinct colocalization (Figure 3A). A subcellular fractionation assay further confirmed the presence of CASP9 in the P100 pellet that did not include COX4I1, a mitochondrial inner membrane protein, cytoplasmic CASP3, a downstream executioner caspase activated by CASP9, and most of the mitochondrial outer membrane (HM). Rather, the P100 CASP9 was associated with endosomal proteins, including RAB7A and M6PR (Figure 3B). Furthermore, the co-presence of CASP9 and RAB7A in the same cellular complex was demonstrated by their co-immunoprecipitation (co-IP). Endogenous (physiologically expressed) CASP9 and RAB7A demonstrated two-way co-IP when precipitated from either a cell extract (Figure 3C) or the P100 subcellular fraction (Figure 3D). It has been established that active RAB7A (RAB7A-GTP) binds to the endosomal membrane and recruits the retromer trimer complex (VPS26-VPS35-VPS29) by interacting with VPS35 and/or VPS26 [17]. The retrieval of cargo proteins into an interaction with their transport carriers on the endosomal membrane precedes and initiates the retrograde pathway, which recycles the M6PR and IGF2R, the major acid hydrolase carriers from the endosomes to the TGN [15]. To better evaluate the significance of the interaction between CASP9 and RAB7A, we assessed potential interactions between CASP9 and M6PR and IGF2R. CASP9 interacts with both cargo proteins, as suggested by their co-IP with CASP9 (Figure 3E,F). Although these interactions may be indirect, they place CASP9 at the endosomal membrane in association with effectors of the endosome-to-TGN transport.

CTSD (cathepsin D) missorting in CASP9-deficient cells

Based on its interactions with RAB7A, M6PR, and IGF2R, CASP9 could potentially have a role in the retrieval mechanism and the subsequent retrograde transport of the MPRs. Fibroblasts prepared from embryos that lacked the two MPRs exhibited a massive missorting of multiple lysosomal enzymes and accumulated undigested material in their endocytic compartments [46–48]. Fibroblasts that lacked either one of the MPRs exhibited a milder phenotype of partial impairment in endosomal sorting [49]. To test if CASP9 deficiency causes defects in IGF2R retrograde transport, we assessed the processing and potential secretion of newly synthesized CTSD, a hydrolase that relies on IGF2R for its lysosomal targeting [46–49]. CTSD is synthesized in a precursor form that subsequently evolves into the intermediate and mature forms upon reaching the acidic milieu of the endosomal and lysosomal compartments. Under normal conditions, CTSD is efficiently sorted by the endocytic system, and little is secreted from the cells. CTSD missorting is indicated by the accumulation of precursor and intermediate CTSD that do not reach the lysosomal acidic milieu required for their maturation or by their secretion from the cells [29]. Such CTSD missorting was observed for cells deficient in components of the endosomal transport complexes, including VPS35, SNX1, and DNAJC13/RME-8 [29,35,50–52]. We observed an accumulation of precursor CTSD in *casp9* KO MEF chased with cycloheximide, as well as in *CASP9* KO HCT116 cells (Figure 4A,B) suggesting that newly synthesized CTSD does not reach the lysosome, where it should be processed into its mature form. Furthermore, the CTSD precursor was mis-transported in both *casp9* KO MEF and *CASP9* KO HCT116 cells, as it was secreted into the culture medium. We also assessed the impact of *CASP9* KD, utilizing *VPS35* KD as a positive control.

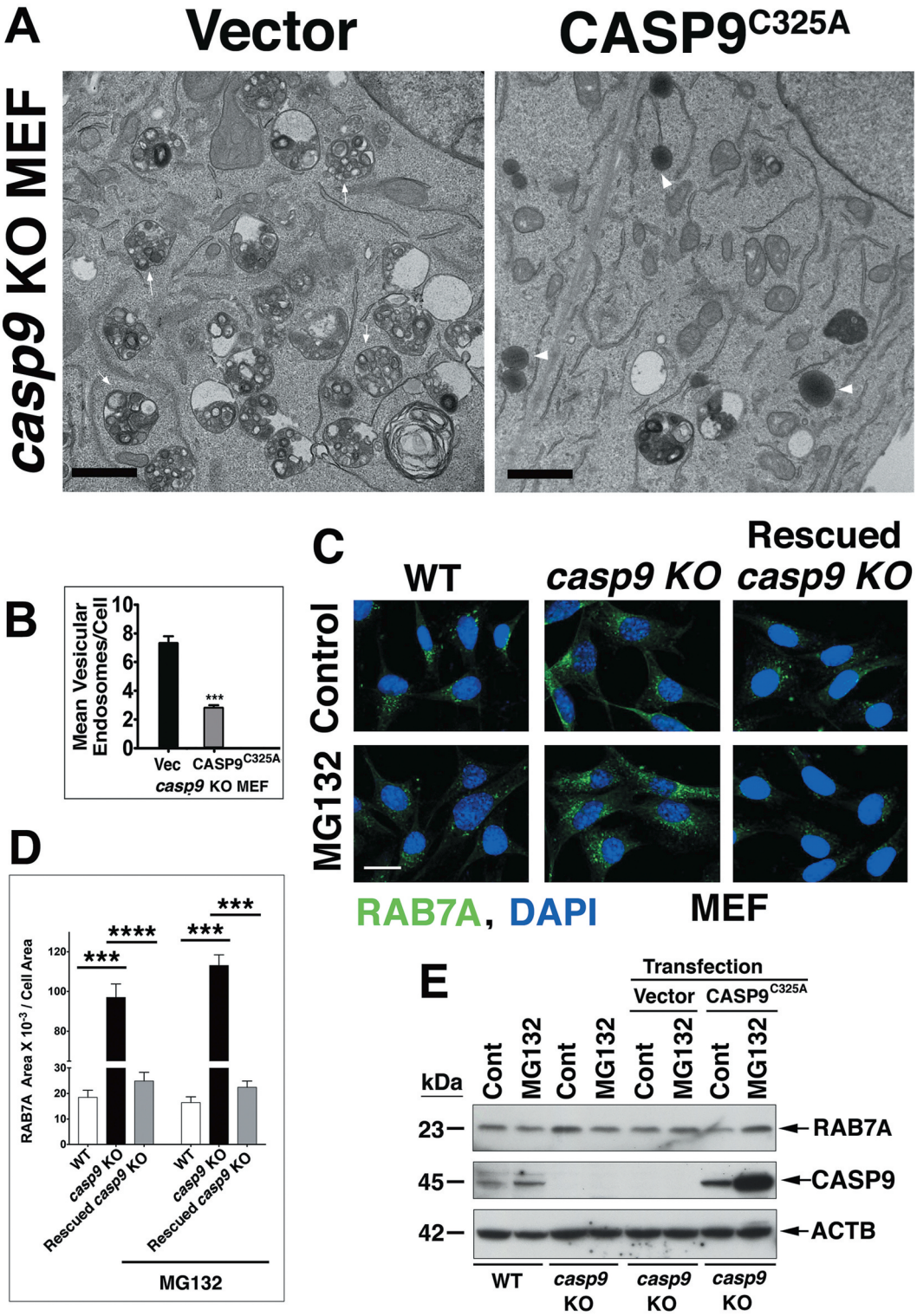

Figure 2. The enhanced accumulation of late endosomes in *casp9* KO MEF cells is reduced by the transfection of a plasmid encoding the non-catalytic CASP9^{C325A} mutant. (A-B) The accumulation of late endosomes in *casp9* KO MEF is significantly reduced following the transfection of CASP9^{C325A}. Scale bars: 500 nm. White arrows indicate few of the endosomes; arrowheads – lysosomes. (B) Quantification of vesicular endosomes. The data are means±SEM of endosomes in 50 cells in each of 3 independent experiments. *** = $p < 0.0001$ (MWU). (C-D) CASP9 expression alters the distribution pattern of RAB7A in control and MG132-treated MEF. WT, *casp9* KO MEF, and *casp9* KO MEF transfected with CASP9^{C325A} were treated with the vehicle or MG132 (1 μM, 16 h) and assessed by a confocal microscope for RAB7A distribution patterns and expression levels. Scale bars: 40 μm. Similar results were obtained with a distinct RAB7A Abs (SC-10,767) that we authenticated against CRISPR-Cas9 *rab7a* KO cells. The data are means±SEM of at least 50 cells in one of three experiments. *** = $p < 0.0001$ (MWU). (E) Immunoblotting of the cell lysates in one of the experiments shown in C.

A similar level of accumulation of the CTSD precursor was detected in either *CASP9* or *VPS35* KD HCT116 cells, representing increased expression levels of the precursor CTSD in comparison to the non-target siRNA control cells (Figure 4C). Additionally, a precursor form of HEXB (hexosaminidase subunit beta), an IGF2R-dependent acid hydrolase, accumulated in both *CASP9* KO HCT116 cells (Figure 4B) and *CASP9* KD HCT116 cells (Figure 4C). We also detected

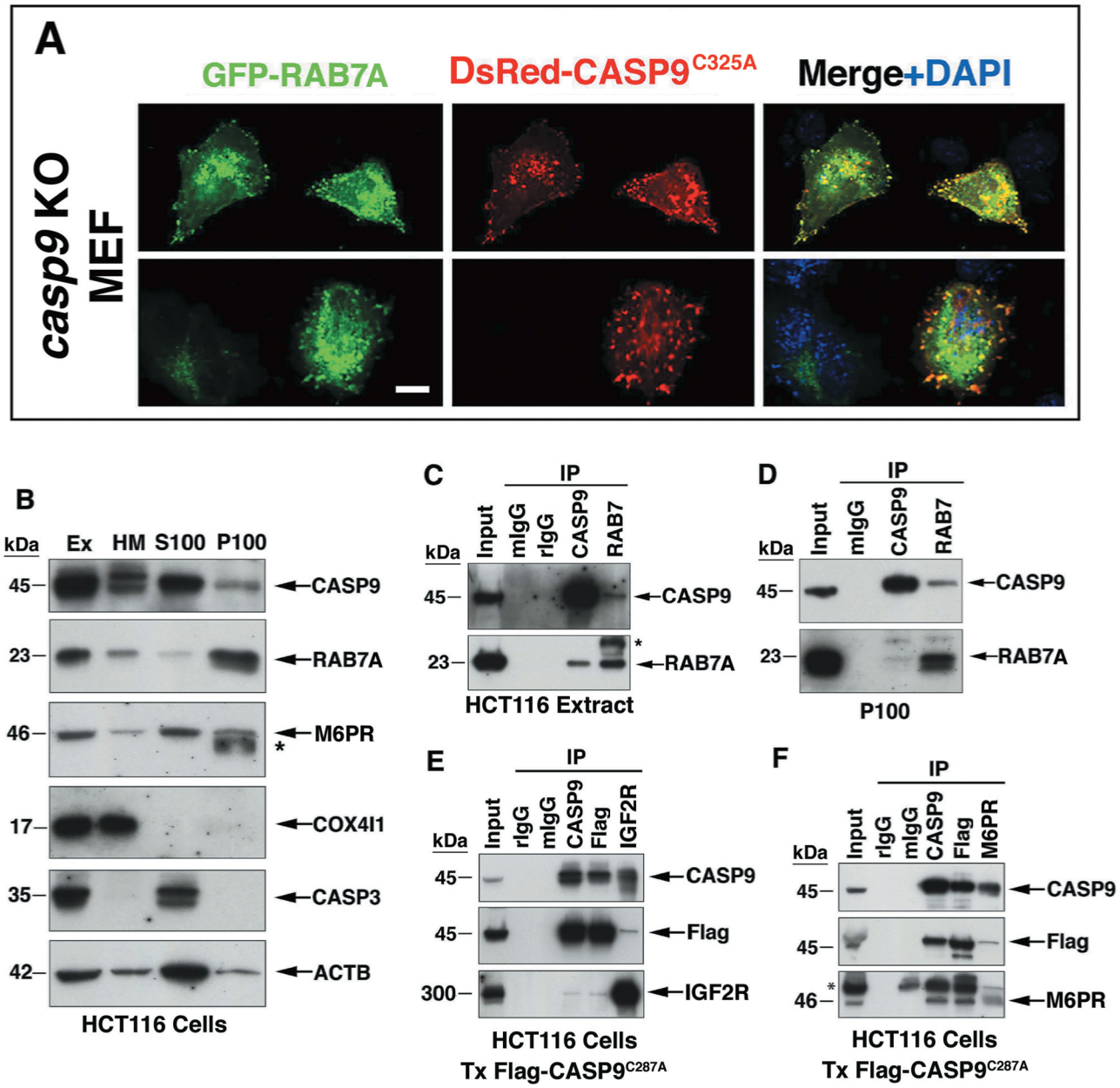

Figure 3. Association of CASP9 with endosomal membrane proteins. (A) Colocalization of GFP-RAB7A and DsRed-CASP9^{C325A} co-transfected into *casp9* KO MEF. A non-transfected negative control cell is included in the bottom panel images. Scale bar: 20 μm. (B) Association of CASP9 with RAB7A and M6PR in the P100 pellet following subcellular fractionation of HCT116 cells. (C-D) Co-IP of CASP9 and RAB7A when immunoprecipitated from HCT116 cell lysate (C) or the P100 subcellular fraction (D). (E-F) Co-IP of CASP9 with IGF2R/CI-MPR (E) and with M6PR (F). The cells were transfected with a plasmid encoding the 3xFlag-CASP9^{C287A} mutant and subjected to IP by anti-CASP9, anti-Flag, anti-IGF2R or anti-M6PR Abs.

reduced GLB1 (galactosidase beta) and GUSB (glucuronidase beta) enzymatic activities in *casp9* KO MEF and reduced GLB1 activity in *CASP9* KO HCT116 cells as compared to their WT counterparts (Figure 4D). To further establish the presence of reduced CTSD activity in CASP9-deficient cells, we utilized a fluorescent inhibitor of CTSD, BODIPY-FL-pepstatin A, that specifically binds to active CTSD [53]. Live staining with this fluorescent inhibitor demonstrated a reduced presence of active CTSD in *casp9* KO MEF as compared to WT MEF, which was significantly rescued by transfection of murine catalytic mutant CASP9^{C325A} (Figure 4E,F). These findings suggest that deficient expression of CASP9 by its KO or KD, in either murine (fibroblasts) or human tumor cells, is associated with the missorting of CTSD and other acid hydrolases that are IGF2R-dependent for their lysosomal delivery.

Interactions of CASP9 with endosomal membrane transport complexes

Multiple previous studies have concluded the importance of VPS35 in the retrograde pathway of IGF2R, identifying a potential interaction of IGF2R and VPS35 [27,28,30,31]. More recently, CRISPR-Cas9 KO of *VPS35* was reported to

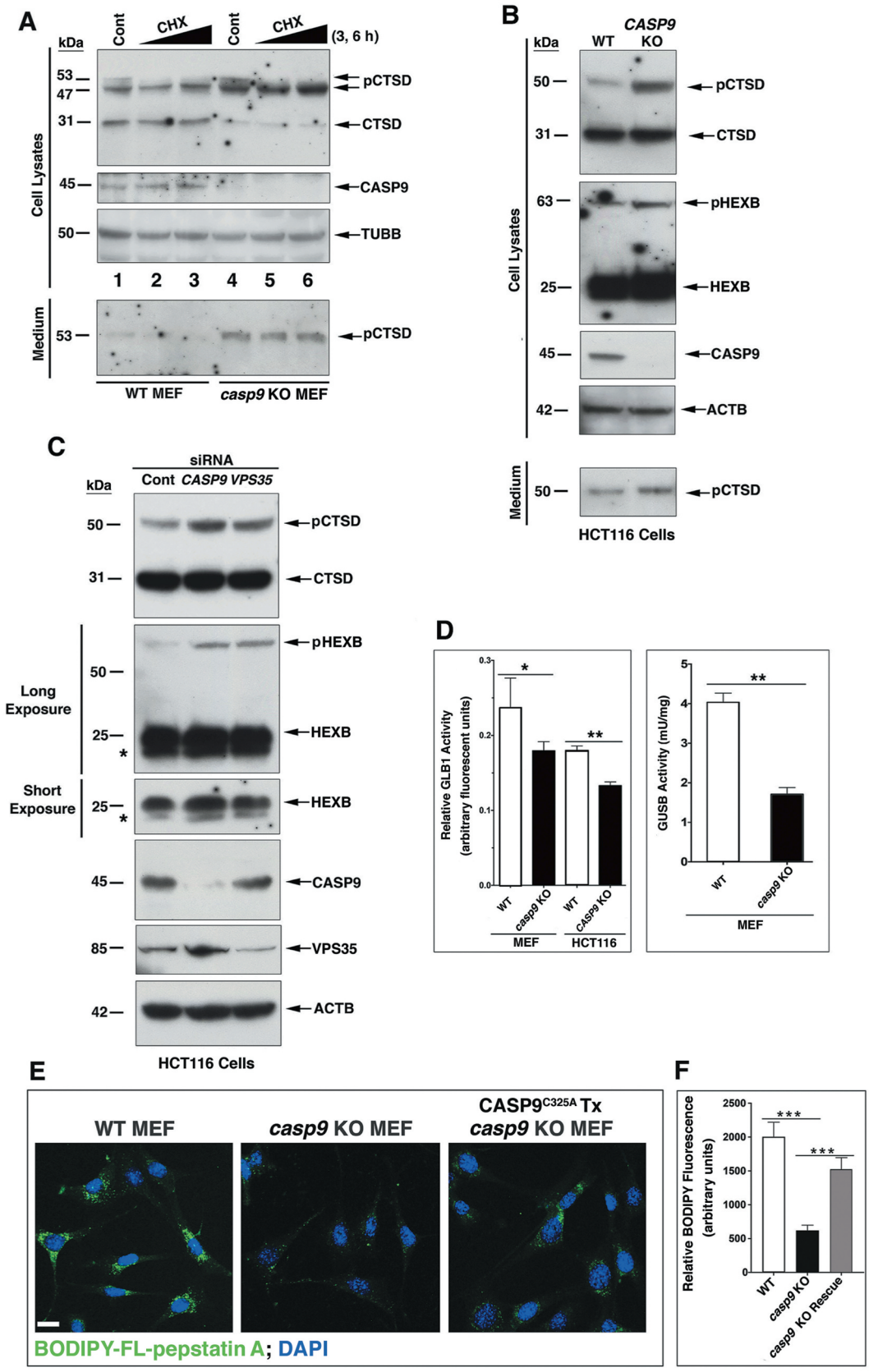

Figure 4. CASP9 expression level impacts the maturation and activation of lysosomal enzymes. (A) Missorting of CTSD in *casp9* KO MEF. WT and *casp9* KO MEF were pre-treated with vehicle control or cycloheximide (CHX, 0.5 μg/ml for 3 or 6 h). Cell lysate and cell culture medium were assessed for the expression of the precursor (pCTSD) and mature forms of CTSD. (B) Missorting of CTSD and HEXB in CRISPR-Cas9 *CASP9* KO HCT116 cells. (C) Accumulation of pCTSD and pHEXB in *VPS35* or *CASP9* KD cells. HCT116 cells were treated with *CASP9* or *VPS35* siRNAs for 48 h and then assessed by immunoblotting for the expression of the indicated proteins. (D) The specific activities of GLB1/galactosidase beta and GUSB/glucuronidase beta are significantly reduced in *casp9* KO MEF as compared to WT MEF. The data are means±SEM of 6 replicates for each group in one of 3 independent experiments with equivalent results. * = $p < 0.05$; ** = $p < 0.001$ (MWU). (E) Differential expression of active CTSD as indicated by live staining with BODIPY-FL-pepstatin A in WT, *casp9* KO, and rescued *casp9* KO MEF. Scale bar: 60 μm. (F) Quantification of live staining with BODIPY-FL-pepstatin A is shown in D. The data are means±SEM of approximately 50 cells in each of 3 independent experiments. *** = $p < 0.0001$ (MWU) .

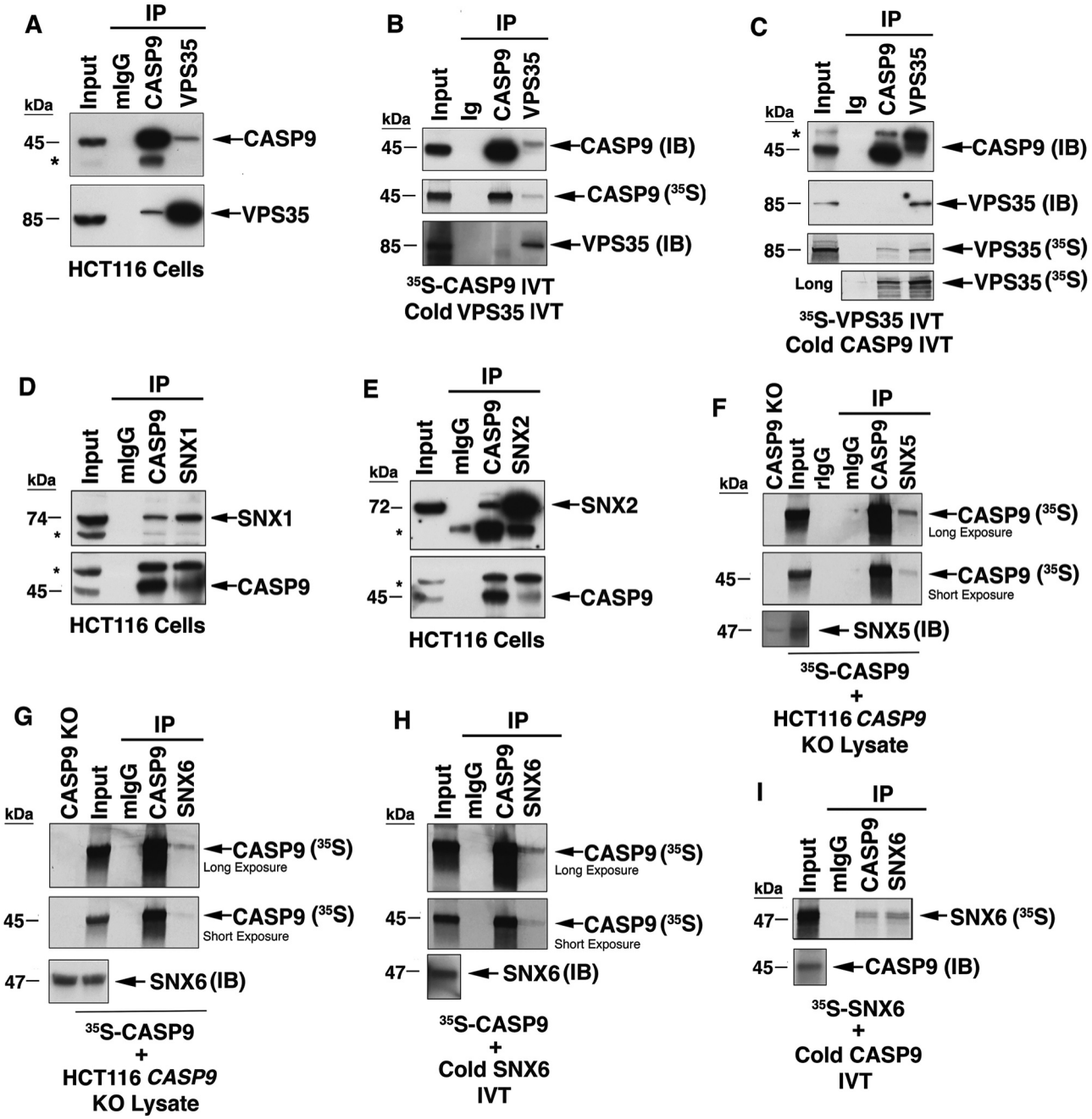

Figure 5. Interaction of CASP9 with endosomal transport complexes. (A) Co-IP of endogenous CASP9 and endogenous VPS35 in HCT116 cells. (B) Co-IP of *in vitro* translated ^{35}S-CASP9 with cold *in vitro* translated VPS35. Input includes the two *in vitro* translated products. (C) Co-IP of *in vitro* translated ^{35}S-VPS35 with cold *in vitro* translated CASP9. (D) Co-IP of endogenous CASP9 with endogenous SNX1 in HCT116 cells. (E) Co-IP of endogenous CASP9 with endogenous SNX2 in HCT116 cells. (F) Co-IP of *in vitro* translated ^{35}S-CASP9 with endogenous SNX5 from HCT116 *CASP9* KO lysate. Input includes lysate of HCT116 *CASP9* KO cells combined with *in vitro* translated ^{35}S-CASP9. (G) Co-IP of *in vitro* translated ^{35}S-CASP9 with endogenous SNX6 from HCT116 *CASP9* KO lysate. Input includes lysate of *CASP9* KO cells combined with *in vitro* translated ^{35}S-CASP9. (H-I) Co-IP of *in vitro* translated ^{35}S-CASP9 with cold *in vitro* translated SNX6 (H), or *in vitro* translated ^{35}S-SNX6 with cold *in vitro* translated CASP9 (I). The immunoblotting of the immunoprecipitated SNX5 and SNX6 in (F-I) are not shown because of the similar gel migration of the co-IP proteins. Inputs include the two *in vitro* translated products.

have no impact on the retrograde transport of IGF2R from the endosomes to the TGN, whereas double KO of *SNX1* and *SNX2* or *SNX5* and *SNX6*, which eliminated both SNX1-SNX5 and SNX2-SNX6 complexes caused the accumulation of IGF2R on EEA1 (early endosome antigen 1)-positive endosomes with a concomitant reduction in IGF2R colocalization with TGOLN2/TGN46 [25,34]. These findings implied that the SNX-BAR proteins are involved in IGF2R-retrieval transport, while the role of VPS35 remains uncertain [33]. To further analyze the specific function of CASP9 in the observed missorting of the lysosomal hydrolases, we assessed for the interactions of CASP9 with the VPS35 and the SNX-BAR complexes. Endogenous CASP9 demonstrated two-way co-IP with endogenous VPS35 when immunoprecipitated from cell lysates (Figure 5A). When precipitated from a mixture of *in vitro* translated CASP9 and VPS35, where either CASP9 or VPS35 were ^{35}S-methionine-labeled, VPS35 IP brought along ^{35}S-CASP9 (Figure 5B), and CASP9 IP brought along

^{35}S-VPS35 (Figure 5C). Endogenous CASP9 further demonstrated two-way co-IP with SNX1 and SNX2 (Figure 5D,E). Through its interaction with SNX1 and SNX2, CASP9 may contact the SNX1-SNX5 or SNX2-SNX6 complexes. In our attempt to assess for the potential interactions of CASP9 with SNX5 or SNX6, a simple endogenous co-IP experiment did not provide clear results due to the comparable molecular masses of CASP9 (45 kDa), SNX5 (47 kDa), SNX6 (47 kDa), and the Ig heavy chain of the IP Abs (~50 kDa). To overcome this issue, we combined *in vitro* translated ^{35}S-CASP9 with a *CASP9* KO cell lysate and subjected the mixture to CASP9 or SNX5 co-IPs (Figure 5F). Immunoprecipitated SNX5 brought along ^{35}S-CASP9. Likewise, IP of SNX6 from the *CASP9* KO cell lysates brought along *in vitro* translated ^{35}S-CASP9 that was added to the cell lysate (Figure 5G). We further assessed the interaction of *in vitro* translated CASP9 and *in vitro* translated SNX6, where only one of the *in vitro* translated products was ^{35}S-methionine-labeled (Figure 5H,I). SNX6 IP brought along ^{35}S-CASP9 and CASP9 IP brought along ^{35}S-SNX6. These potential interactions of CASP9 were also indicated by its colocalization with VPS35, SNX1, and SNX2, as assessed by confocal microscopy (**Fig. S5**). Overall, our co-IP and colocalization results suggest that CASP9 interacts (directly or indirectly) with the retromer trimer via its interaction with VPS35, and also with the SNX dimers, including SNX1-SNX5 and SNX2-SNX6. These findings place CASP9 on the endosomal membrane in association with the two endosomal transport complexes – the retromer and the SNX dimers that are involved in the IGF2R retrograde transport pathway(s) [25,26,33–35].

Impact of CASP9 on the IGF2R expression level

With abrogated retrograde transport, endosomal IGF2R is eventually degraded. A reduced IGF2R expression level has been detected in cells deficient in retromer components [27–29], but these findings have not been consistently corroborated [23,30]. To further investigate the crosstalk between CASP9 and the MPRs, we tested the impact of *CASP9* KD or KO on the expression levels of M6PR and IGF2R. Using confocal microscopy, we observed a striking reduction in the expression level of IGF2R in CASP9-deficient cells (Figure 6A,B**, and S6**) but did not detect a significant impact on the M6PR expression level (**Fig. S6**). The dependence of IGF2R, but not M6PR expression levels on CASP9, was also confirmed by immunoblotting of HCT116 cells treated with *CASP9* siRNA (Figure 6C). Furthermore, the IGF2R expression level was markedly reduced in both CRISPR-Cas9 *CASP9* KO A549 or HCT116 clonal cell lines and rescued in the presence of BafA1 (Figure 6D-F). In contrast, the expression level of M6PR did not demonstrate dependence on either CASP9 or BafA1. The BafA1-mediated rescue of IGF2R expression suggests that in the absence of CASP9, IGF2R is directed to a lysosomal degradation pathway. As IGF2R degradation is expected to yield impaired lysosomes, we tested the possibility that the proteasomal system also contributes to the observed IGF2R reduced expression. Indeed, IGF2R is degraded by both the proteasomes and lysosomes since treatments by either BafA1 or MG132 elevate its expression level both in WT and *CASP9* KO cells (Figure 6D-G). To further validate the dependence of IGF2R on CASP9, we transfected *CASP9* KO A549 cells with vector control, WT CASP9, or the non-catalytic CASP9^{C287A} mutant (Figure 6H). Transfection of either WT or catalytically inactive CASP9 enhanced the expression level of IGF2R in *CASP9* KO cells. Importantly, plasmids encoding non-catalytic CASP9 mutants, such as murine CASP9^{C325A} or human CASP9^{C287A} transfected into the appropriate *casp9*/*CASP9* KO cells, have no dominant-negative effect, since these cells do not express CASP9. These findings suggest that endosomal CASP9 deficiency enhances the degradation of IGF2R, potentially diminishing its retrieval to the retrograde transport.

Association of CASP9 with the endosomal degradative subdomain

Endosomes serve as the sorting hub for multiple cargoes that are directed to either degradation or retrieval mechanisms [54]. Cargoes that are destined to degradation are usually sorted by the ESCRT family into endosomal intraluminal vesicles (ILVs) [55]. Cargo-loaded ILVs fuse with the lysosomes, generating endolysosomes that, following cargo degradation, give rise to the re-formed lysosomes [56]. The initial linking to the ESCRT machinery occurs on an endosomal degradative subdomain characterized by the presence of HGS/ESCRT-0/HRS, which is stabilized and concentrated by flat clathrin via its interaction with the CLTC (clathrin heavy chain) [23,57]. To assess the potential involvement of CASP9 in a crosstalk mechanism between the retrieval and the degradative subdomains, we tested for the interactions of CASP9 with HGS and CLTC. As determined by co-IP, endogenous CASP9 interacts with both components of the endosomal degradative domain (Figure 7A,B). We also observed the colocalization of transduced DsRed-CASP9^{C325A} with endogenous CLTC (Figure 7C). Of note, the interaction between CASP9 and CLTC has been previously identified in a proteomic search for CASP9-interacting proteins [58]. Interestingly, *CASP9* KO cells demonstrated an increased expression of HGS as compared to their WT counterparts, and transfection of CASP9 reduced the HGS expression level, suggesting functional crosstalk between HGS and CASP9 (Figure 7D). Likewise, while overexpression of CASP9 resulted in a downregulated expression of CLTC (Figure 7E), *CASP9* KD resulted in the upregulated expression of CLTC (Figure 7F), also suggesting the existence of a dynamic crosstalk mechanism between CASP9 and clathrin. These findings suggest that endosomal proteins that initiate the degradation process on the degradative endosomal subdomain are also impacted by the expression level of CASP9. Potentially, overexpression of CASP9, which appears to enhance the retrieval mechanism, concurrently reduces the CLTC available for the degradative subdomain, while a reduced expression level of CASP9, which is associated with increased IGF2R degradation, requires the stabilization of the degradative subdomain by increased expression of CLTC. Based on these findings, we propose that endosomal CASP9 negatively regulates the formation of an active degradative endosomal subdomain, thereby blocking the lysosomal degradative path for IGF2R.

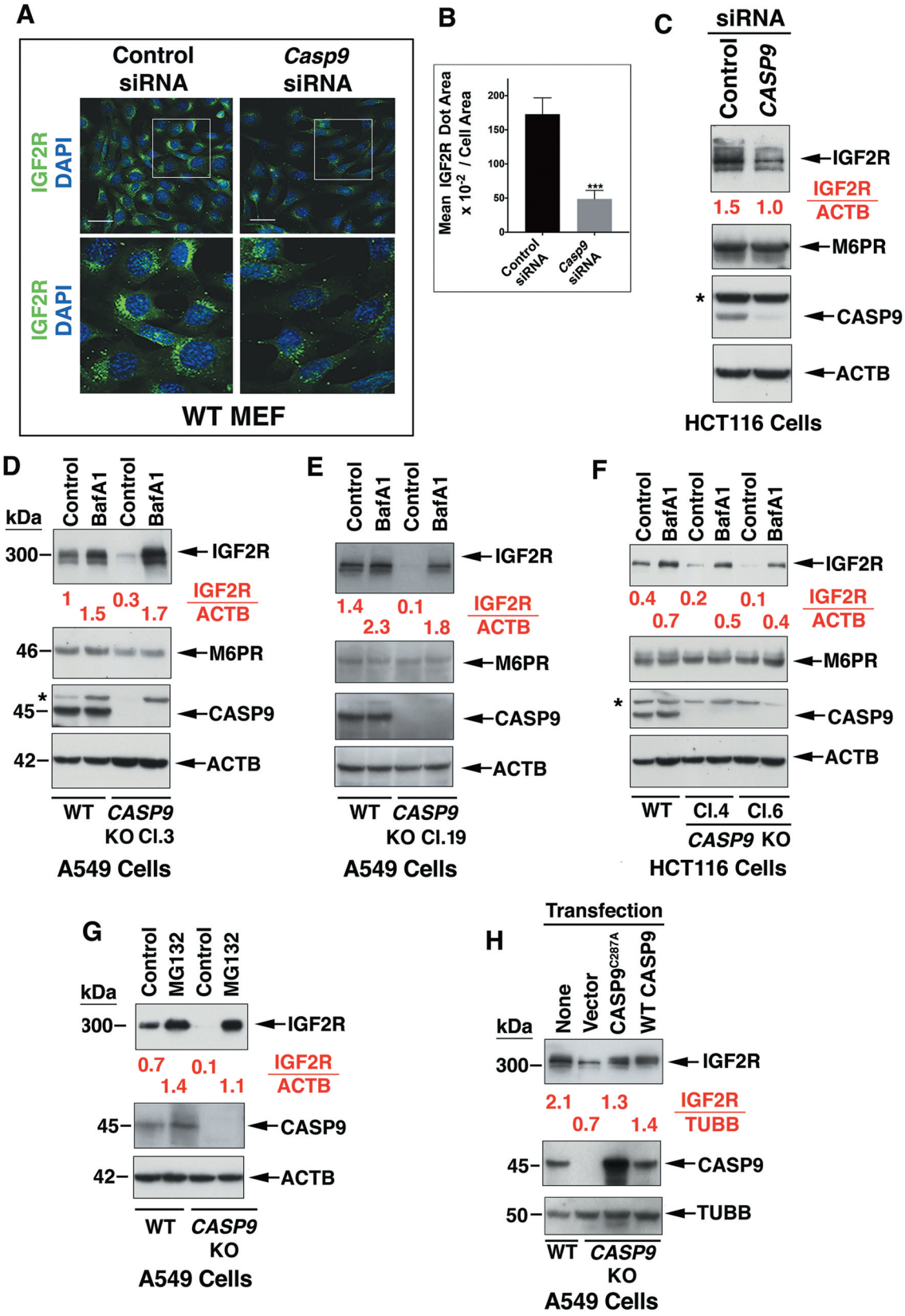

Figure 6. Degradation of IGF2R in *CASP9* KO clonal cell lines is rescued by BafA1, MG132, or re-expression of either WT or non-catalytic CASP9^{C287A} mutant. (A) *Casp9* KD reduces the expression of IGF2R significantly, as determined by confocal microscopy. Scale bar: 100 µm. (B) Quantification of results shown in A. The data are means±SEM of at least 40 cells per treatment in 3 independent experiments. *** = $p < 0.0001$ (MWU). (C) *CASP9* KD reduces the expression of IGF2R as assessed by immunoblotting. (D-F) The reduced expression of IGF2R in CRISPR-CAS9 *CASP9* KO clonal cell lines (A549 clones 3 and 19; HCT116 clones 4 and 6; Cl.: clone) is rescued in the presence of BafA1. A549 CRISPR-Cas9 *CASP9* KO clones (3 and 19) were generated by distinct gRNAs. (G) The reduced expression of IGF2R in *CASP9* KO A549 cells is rescued by treatment with MG132 (1 µM, 16 h). (H) The reduced expression of IGF2R in *CASP9* KO A549 cells is rescued by transfection of plasmids coding for either WT or non-catalytic CASP9^{C287A} mutant.

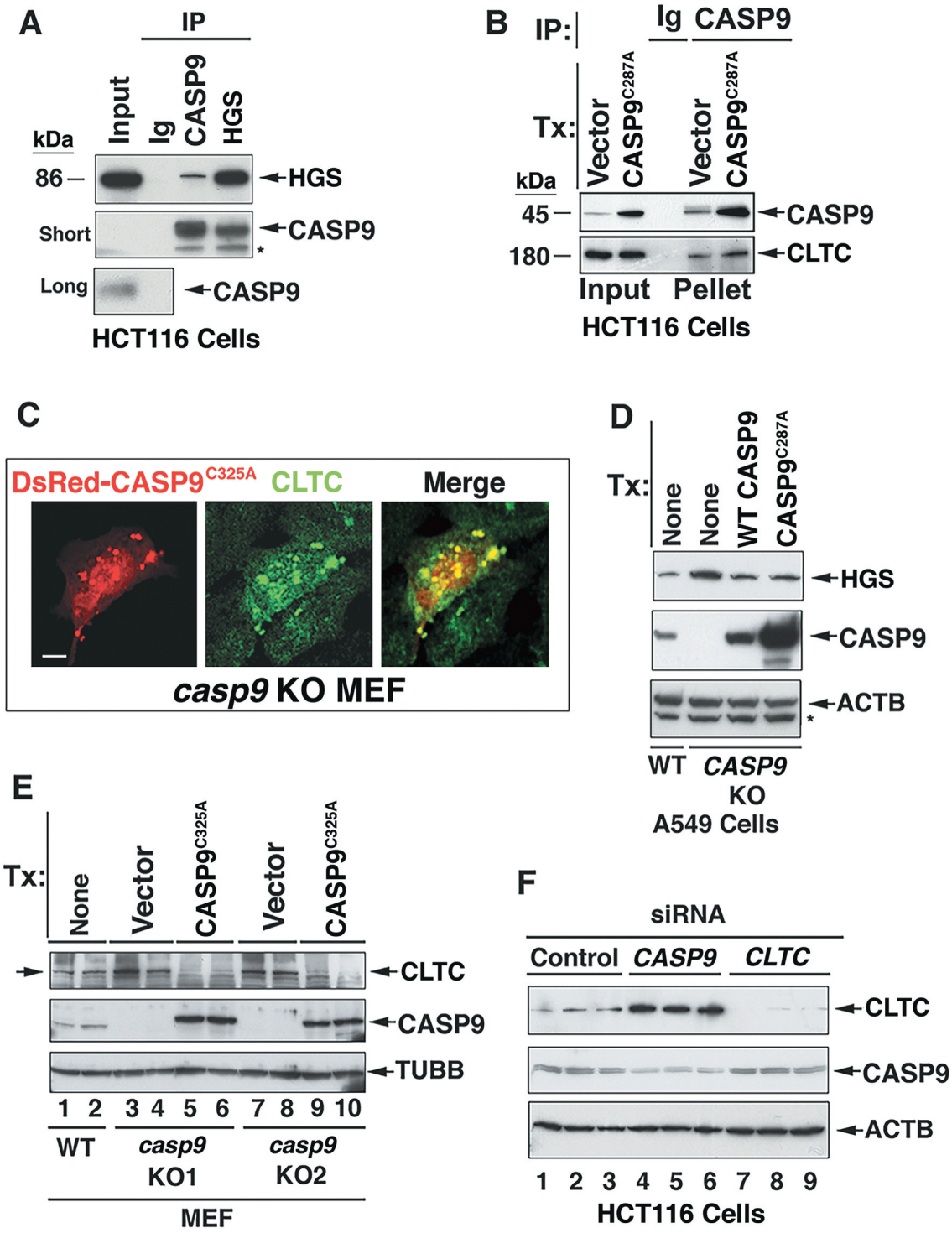

Figure 7. CASP9 interacts with the endosomal degradative subdomain proteins HGS and CLTC and alters their expression levels. (A) Co-IP of physiologically expressed CASP9 and HGS. (B) Co-IP of CLTC with either physiologically expressed CASP9 (vector control) or catalytically inactive CASP9^{C287A} mutant in stably transfected in HCT116 cells. (C) Colocalization of DsRed- CASP9^{C325A} with endogenous CLTC. CLTC was detected by rabbit anti-CLTC and Alexa Fluor 488 anti-rabbit Abs. Scale bar: 10 μm. (D) The increased expression of HGS in *CASP9* KO cells is reduced by the overexpression of WT or catalytic CASP9^{C287A} mutant. (E) Overexpression of the gene encoding the non-catalytic CASP9^{C325A} mutant in *casp9* KO MEF reduces the expression of CLTC. Lanes 1,3,5,7,9 were treated with vehicle control and lanes 2,4,6,8,10 with MG132 (1 μM, 16 h). To simplify the presentation, the control and MG132 treatments are not indicated in the figure. (F) Upregulation of CLTC in response to *CASP9* KD. HCT116 cells were treated with non-target control (lanes 1–3), *CASP9* (lanes 4–5), or *CLTC* (lanes 7–9) siRNAs. Lanes 1,4,7 were treated with vehicle control; lanes 2,5 and 8 were treated with MG132, and lanes 3,6,9 were treated with bortezomib (100 nM, 16 h). To simplify the presentation, the proteasome inhibitors (that did not impact the expression levels of CASP9 or CLTC) are not indicated on the figure.

Discussion

The current study has identified an unexpected player – CASP9 – in the molecular crosstalk between endosomal subdomains that determine the retrieval or degradation of IGF2R. Notwithstanding the surprising nature of this discovery, the evidence for placing CASP9 at the endosomal membrane is substantial. In essence, endogenous CASP9 interacts, in either a direct or indirect manner, with multiple components of the endosomal transport mechanism. Most of these interactions are demonstrated by confocal colocalization, and further, by two-way co-immunoprecipitation between physiologically expressed CASP9, and physiologically expressed endosomal proteins. The unexpected locality of the endosomal membrane for the identified non-apoptotic activity of CASP9 potentially enables its exclusion from the cytosolic apoptosome triggered by the mitochondrial-released cytochrome c and ensures distinct cellular localizations between its apoptotic and non-apoptotic activities. Not only the distinct cellular localizations but also post-translational modifications of CASP9, such as ubiquitination or phosphorylation, may determine its apoptotic vs. non-apoptotic cellular contribution; however, this issue requires further investigation. The significance of the interactions of CASP9 with endosomal proteins is indicated by the negative impact that CASP9 deficiency exerts on endosomal maturation and lysosome quality in an array of cells, including murine normal fibroblasts and human tumor cells. The reduced lysosomal capability of CASP9-deficient cells is indicated by the impaired lysosomal transport of acid hydrolases known to be IGF2R-dependent, reduced lysosomal degradative efficiency for BafA1-sensitive proteins, and a reduced capability as compared to CASP9-expressing cells, in compensating for proteasomal inhibition by enhanced lysosomal degradation of ubiquitinated proteins.

The ubiquitin-proteasome system (UPS) and lysosomes (in service of either autophagy or endocytic transport) are the two major degradative systems in eukaryotes. The UPS is responsible for the degradation of short-lived proteins and soluble misfolded proteins, whereas autophagy degrades insoluble protein aggregates or impaired organelles. A compensatory relationship between the two systems was revealed by the use of specific inhibitors [38–40]. Thus, a defect in one of the two degradation systems has led to upregulation in the other [40]. Ubiquitination commonly serves both systems in directing substrates to the proper degradation pathway but also mediates interconnections that allow the shifts between the two systems [40]. In the current study, deficiency in CASP9 inhibited the ability of the lysosomal system to compensate for the inhibition of the UPS by the proteasome inhibitor, MG132. Thus, the upregulation of autophagic activity, previously demonstrated for multiple UPS inhibitors (MG132, bortezomib, lactacystin, etc.) [40], was negated in the absence of CASP9. In the same vein, deficiency in CASP9 increased the overall degradation of IGF2R, but it was now mediated by both lysosomal and proteasomal activities.

The interaction of CASP9 with endosomal proteins is distinctive, as it interacts with endosomal proteins involved in the IGF2R retrieval toward the retrograde transport, as well as with those involved in the IGF2R degradation. It has been demonstrated that endosomes contain large non-overlapping membrane microdomains [59], including those that are marked by HGS and clathrin and are separated from those marked by EEA1 [23,24,60]. In line with a potential separation between retrieval and degradative subdomains [54,61], we propose that CASP9 carries out a crosstalk(s) with VPS35, SNX1, SNX2, SNX5, SNX6, and RAB7A on the retrieval subdomain that complements its impact on HGS and CLTC on the degradative subdomain (Figure 8). CASP9 interaction with these functionally opposing endosomal subdomains impacts their dynamics. Thus, CASP9 alters the expression pattern of RAB7A, which is involved in both the retromer and the SNX dimer recruitment to the endosomal membrane. To initiate a retrieval activity, active endosomal RAB7A (GTP-bound) recruits the retromer to the endosomal membrane [17], while the PX domain present in both SNX1/2 binds PtdIns3P to recruit the SNX dimers to the endosomal membrane [62]. As indicated, PtdIns3P is generated by PtdIns3K (also known as VPS34/PIK3 C3), which is an indirect interactor with RAB7A-GTP, and is dependent on RAB7A's nucleotide cycling activity for its kinase activity [19]. It is, therefore, possible that CASP9-mediated changes in the cellular distribution of RAB7A affect the latter's ability to recruit the retromer or the SNX dimers to the endosomal membrane.

On the degradative subdomain, CASP9 interacts with and alters the expression levels of HGS and CLTC. In contrast to other studies that have investigated the TGN vs. the endosomal ends of the retrograde pathway, our study focused on two contrasting endosomal functions: degradation on the one hand, and rescue from degradation (retrieval) on the other. CASP9 appears to be involved in these two opposing endosomal mechanisms that determine the outcome for IGF2R: being degraded or retrieved. The interactions of CASP9 with endosomal transport complexes indicate its specific involvement in the IGF2R transport by these complexes. However, the exact molecular mechanism utilized by CASP9 to enhance IGF2R retrieval for the retrograde transport remains unknown and requires further investigation. The identified crosstalk between CASP9 and components of the degradative subdomain suggests an active involvement of CASP9 in the dynamics of the degradative endosomal subdomain. Substantial evidence suggests that clathrin is recruited to the endosomal membrane by HGS and that it is required for efficient ILV formation and eventual cargo degradation [23,24]. Our results place CASP9 not only at the retrieval endosomal subdomain but also at the degradative subdomain, where it impacts the expression level of HGS and the recruitment level of CLTC. The interactions of CASP9 with components of both the retrieval and degradation pathways for IGF2R suggest that while enhancing IGF2R retrieval, CASP9 inhibits its degradation. The efficient IGF2R degradation observed in conjunction with complementary changes in the expression of HGS and CLTC upon CASP9 deletion, together with concomitant changes in RAB7A dynamics, suggests that CASP9 functions on both ends of the crosstalk occurring between the opposing endosomal subdomains, thus contributing to the selection between IGF2R retrieval and degradation.

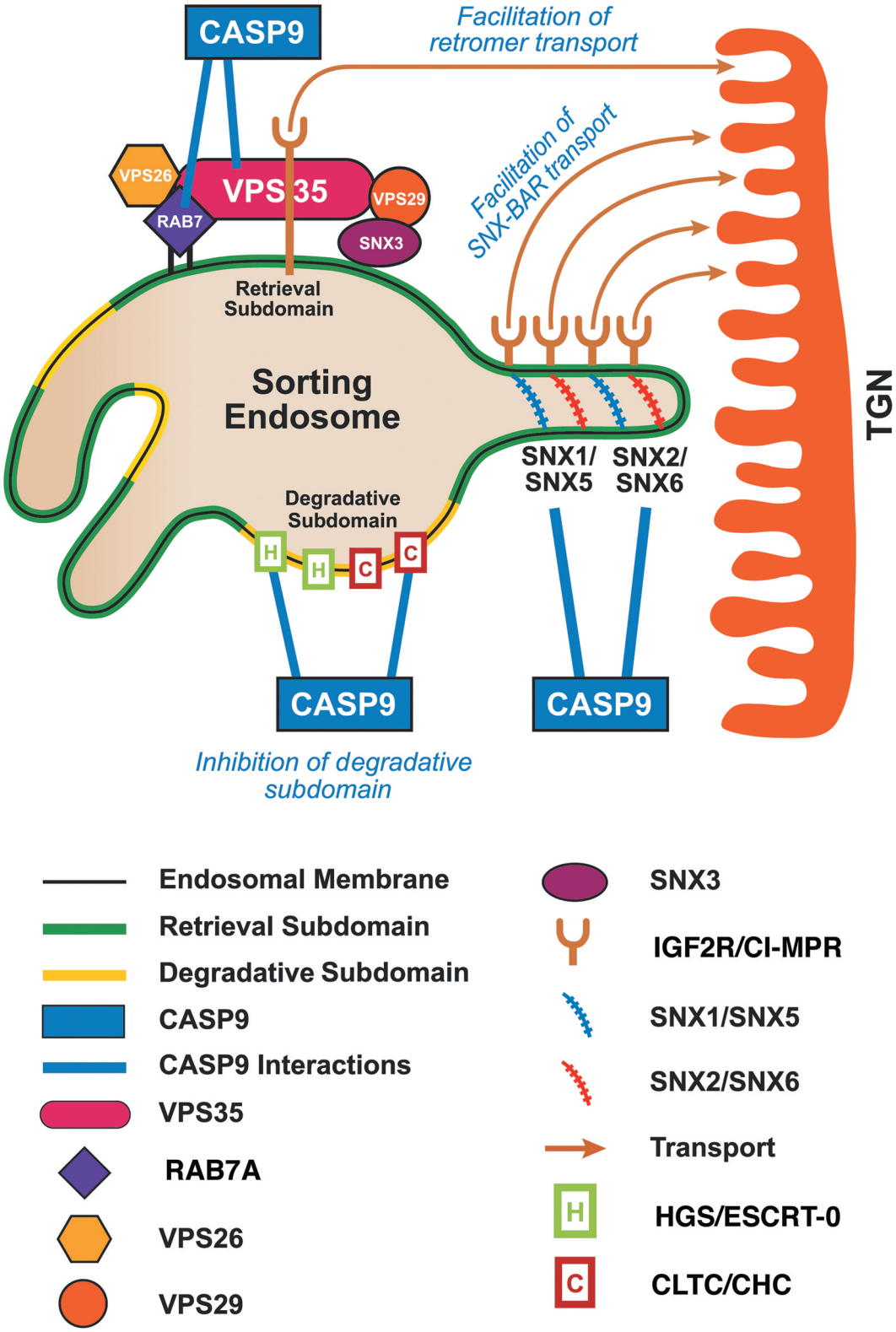

Figure 8. A model illustrating the interactions of CASP9 with components of the endosomal degradative subdomain (HGS, CLTC) and with the retrieval subdomain (retromer or SNX-BAR complexes) that regulate the retrograde transport of IGF2R from endosomes to the TGN.

The non-apoptotic activity of CASP9 on the degradative endosomal subdomain appears to resemble the endosomal activity of DNAJC13 that interferes with the organization of endosomal clathrin and ESCRT to prevent cargo from sorting toward degradation [61]. The interaction of DNAJC13 with SNX1 provides a mechanism for the segregation between the SNX dimer-containing subdomain and the ESCRT/CLTC subdomain [22]. As indicated, loss of either CASP9 or DNAJC13 results in cargo missorting and impaired lysosomal activity, as reported for components of the IGF2R retrieval

mechanism, including the retromer (VPS35 and VPS26) and SNX-BAR (SNX1 and SNX6) [30,63,64].

The degradation of IGF2R in *CASP9* KO cells is likely to be tied to the observed missorting of the acid hydrolases in CASP9-deficient cells. This missorting is expected to impact the quality of the lysosomes formed under such conditions, thus explaining the harnessing of the proteasomal system for the effective degradation of IGF2R.

Materials and methods

Reagents

CASP9 Abs included Santa Cruz Biotechnology (SC) sc-8355 and sc-7885 (immunoblotting) and sc-17784 (immunostaining). Additional SC Abs included TUBB (tubulin beta) sc-9104; ACTB (actin beta) sc-47778; and ubiquitin sc-8017. RAB7A Abs included sc-376362 (immunoblotting), Abcam ab214806 and sc-10767 (staining and immunoblotting), and Cell Signaling Technology 9367 (immunoblotting). VPS35 Abs included sc-374372 (staining and immunoblotting), and Novus Biologicals NB100-1397 (immunoblotting). SNX1 Abs included sc-376376 (staining) and sc-292684 (immunoblotting). Additional anti-SNX Abs included SNX2 sc-136072 (staining and immunoblotting); SNX5 Abcam ab180520; and SNX6 sc-365965. LAMP2 Abs included ABL-193 from Developmental Studies Hybridoma Bank (DSHB http://dshb.biology.uiowa.edu); mouse sc-18822 and rabbit sc-5571 (staining and immunoblotting). M6PR Abs included 22d4 from DSHB, Abcam ab134153 and sc-365196 (staining and immunoblotting). Additional Abs included HEXB (hexosaminidase beta) sc-376781; IGF2R/CI-MPR Abcam ab124767 (staining and immunoblotting); COX4I1 4844 and CLTC 2410 from Cell Signaling Technology; and FLAG 3165 from Sigma. CTSD Abs included human-specific AF1014 Ab and mouse-specific AAF1029 Ab from RD Systems. Fluor 488 or 594 conjugated anti-rabbit or anti-mouse Ig were from Alexa (A11008 and A11005). Pepstatin A, MG132, and DAPI were from Sigma (P5318, 474790, D9542); E64D was from Calbiochem (324890); BODIPY FL-pepstatin A was from Invitrogen (p12271). Plasmids from Invitrogen included pCR3.1 (K3000-01); pcDNA4/TO, pcDNA4/TO/lacZ (V1020-20); and pcDNA6/TR (V1025-20).

Plasmids

Generation of expression plasmids for mouse CASP9^{C325A}, mouse N-terminal 3X Flag CASP9^{C325A}, human WT CASP9, and CASP9^{C287A} were previously described [1]. Human N-terminal *3X Flag CASP9^{C287A}* was produced using the human *CASP9^{C287A}* plasmid as the template for PCR with the following two primers: 5′- CGCGGATCCGCCATG GACTACAAAGACCATGACG TGATTATAAAGATCATGACATCGATTACAAGGATGACG-ATGACAAG ATGGACGAAGCGGATCGG-3′ (forward) and 5′-ACGCGTCGACTGCAA GATAAGGCAGGGTGAG-3′ (reverse). All other reaction conditions and processing were as previously described [1]. Mouse DsRed-monomer CASP9^{C325A} was generated using the above-described mouse CASP9^{C325A}-encoding plasmid as a template for PCR using the following primers: 5′-ACGCGTCGACATGGACGAGGCGGACCGGCAG-3′ (forward) and 5′- CGGGGTACCCTTCGGAGAGAATA ATGAGGC-3′ (reverse). The mutant *casp9* amplicon was purified, digested with restriction endonucleases KpnI and SalI (New England Biolabs) and ligated to the pDsRed-Monomer-Hyg-C1 vector (Clontech, 632495) also predigested with KpnI and SalI, all as described for the CASP9^{C325A} construct above. Randomly picked putative DsRed-monomer *Casp9^{C325A}* clones were sequenced by the University of Pittsburgh Genomics and Proteomics Core Laboratories for sequence verification. The *VPS35* plasmid used for *in vitro* translation was obtained from Dharmacon (MHS6278-202806093;IMAGE iD 30340379). The *SNX6* plasmid utilized for *in vitro* translation was from the Harvard Plasmid Repository (HSCD00452472). *pDest-EGFP-Rab7a* plasmid was previously described [65]. The CRISPR-Cas9 plasmid for human *RAB7A* KO was from Sigma (HSPDD000046457).

Cell lines

A549 cell lines were obtained from ATCC (CCL-185). The HCT116 cell line was obtained from Bert Vogelstein (The Ludwig Center at Johns Hopkins). HCT116 cells expressing CASP9^{C287A} or 3XFlag-CASP9^{C287A} were previously described [1]. WT and *casp9* KO MEF (I and II) were obtained from Richard Flavell (Yale University) and Tak W. Mak (University Health Network, Toronto, Ontario, Canada), respectively. Tumor cell lines and WT or *casp9* KO MEF were grown in Dulbecco's modified Eagle's medium (Invitrogen, 11965092) containing 10% fetal calf serum (Invitrogen, 26140079), 20 mM L-glutamine (Invitrogen, 25030164), and 100 units/ml each of penicillin and streptomycin (Invitrogen, 151401220).

Transfection

Transfections were carried out with Lipofectamine 3000 (Invitrogen, L3000015) according to the manufacturer's instructions using non-linearized plasmids for transient expression and linearized plasmids for stable expression. All procedures involving linearization, transfection, and stable clone selection were carried out as we previously described [66,67].

Generation of CRISPR-Cas9 KO cells

CASP9 KO cells were generated using the GeneArt CRISPR Nuclease Vector with OFP (orange fluorescent protein) Reporter Kit (Invitrogen, A21174), as we previously described [2]. This expression vector system contains both a Cas9 nuclease expression cassette and a guide RNA (gRNA) cloning cassette to generate the target-specific CRISPR RNA. The following two distinct *CASP9* target-specific (Exon2) double-stranded oligonucleotides (Invitrogen) were generated and ligated to the linearized GeneArt CRISPR nuclease vector following the included kit instructions:

Site1: Top Strand – 5′- ACACCCAGACCAGTGGACA TGTTTT- 3′; Bottom Strand – 5′- ATGTCCACTGGTC

TGGGTGTCGGTG – 3′; and Site2: Top Strand – 5′-ACCAGAGATTCGCAAACCAGGTTTT – 3′; Bottom Strand – 5′- CTGGTTTGCGAATCTCTGGTCGGTG – 3′.

Following transformation (*Escherichia coli* DH5a; Invitrogen) plasmids from randomly picked colonies underwent DNA sequence analysis (University of Pittsburgh Sequencing Core Facility) to confirm gRNA sequence integrity.

RNAi

CASP9 siRNAs were obtained from Dharmacon as the siGENOME SMARTpool, which consists of 4 nonoverlapping siRNAs. The matching negative control from Dharmacon was the siGENOME Non-Targeting siRNA Pool 2. Additionally, 3 distinct *CASP9* siRNAs were obtained from Invitrogen as the Stealth Select RNAi *CASP9* Set along with their matching negative controls – the Stealth RNAi Negative Controls LO and Hi GC. All RNAi results obtained by the Dharmacon siGENOME SMARTpool were confirmed by at least an additional distinct *CASP9*-specific siRNA. The cells were plated in a 6-well plate and following 16 h (at 20% confluence) were transfected with 25–100 nM siRNA in Opti-MEM medium (Invitrogen, 31985070) without fetal calf serum using oligofectamine reagent (Invitrogen, 12252011) according to the manufacturer's transfection protocol. After 4 h, fetal calf serum was added to a final concentration of 10%.

Immunoblotting and immunoprecipitation

Cell lysates were prepared with 1% Nonidet P-40 (Sigma, N6507), 20 mM Tris-HCl, pH 7.4 (Bio-Rad, 1610716), 137 mM NaCl (Fisher Scientific, BP358212), 10% glycerol (Fisher Scientific, 15514011), 1 mM PMSF (phenylmethylsulfonyl fluoride, Fisher Scientific, 36978), 10 μg/ml leupeptin (Sigma, L3884), and 10 μg/ml aprotinin (Sigma, A1153). The immunoblotting and immunoprecipitation procedures were described in our previous publications [66–69]. All immunoprecipitation procedures were controlled by a sham procedure with nonspecific matching immunoglobulin. Quantification of scanned protein bands was performed by the US-SCAN-IT Gel software (Version 7.1 for Windows. Silk Scientific, Inc. P. O. Box 533 Orem, UT 84059 USA).

Filter-Trap assay

The assay was performed as previously described [42]. A total cell lysate in SDS lysis buffer (10 mM Tris pH 8.0, 150 mM NaCl, 2% SDS (Bio-Rad, 1610302), 10 μg/ml PMSF (Fisher Scientific, 36978) and 10 μg/ml pepstatin A (Sigma, P5318) was fractionated by centrifugation at 16,000 g. The supernatants were removed and the pellets were resuspended in equal volumes of lysis buffer. Equal volumes of total cell lysate, supernatant and pellet fractions were then analyzed by western blot or filter-trap assay. All pellet fraction samples underwent a further 1:3 dilution in 2% SDS before vacuum filtration through a 96-well dot-blot apparatus (Bio-Rad, 1706543) containing 0.45 μm nitrocellulose membranes (Bio-Rad, 1620115). The resultant membranes were washed twice with 2% SDS wash buffer and immunoblotted as described for western blots. Filter-trap equal loading was ascertained by equal ACTB expression in the immunoblotting of matching supernatants.

BafA1-sensitive protein degradation

The assay was based on a previously described method [70]. The cells were incubated for 24 h at 37°C with 0.2 mCi/ml L-[^{14} C] valine (PerkinElmer, NEC291EU050UC). The cells were washed 3 times with PBS (Fisher Scientific, 17516F) and transferred to fresh complete medium containing 10 mM cold valine (Sigma, V0500) for 1 h. The medium was then replaced with fresh medium containing 10 mM cold valine, in which the cells were treated with vehicle or 100 nM BafA1 for 5–16 h. At the end of the incubation period, the culture medium was subjected to precipitation in 10% trichloroacetic acid (TCA, Sigma, T9159) at 4°C, and the radioactivity of the supernatant (released amino acids) was determined by liquid scintillation counting. The cells were washed twice with cold TCA and dissolved in 0.2 M NaOH. Protein degradation was determined by the ratio of acid-soluble radioactivity in the medium to total radioactivity recovered from both medium and cell pellet fractions.

Cell microscopy and image acquisition

Confocal images were obtained with a confocal laser scanning microscope (Olympus, FV1000) and the companion software FV10-ASW1.6. Images were acquired with the use of the same setting at a resolution of 1020 × 1024 pixels. Morphometric measurements were performed using Metamorph (Universal Imaging) on at least 50 cells per condition.

For transmission electron microscopy, cells were fixed with 2% paraformaldehyde and 2% glutaraldehyde in 0.1 M phosphate buffer (pH 7.0), followed by 1% OsO_4. After dehydration, thin sections were stained with uranyl acetate and lead citrate for observation under a JEM 1011 CX electron microscope (JEOL, Peabody, MA). At least 50 cells per treatment were utilized for quantification of all digitally acquired microscopic images.

Subcellular fractionation

Cells were suspended in the mitochondrial buffer (MIB) composed of 0.3 M sucrose (Sigma, S7903), 10 mM MOPS, 1 mM EDTA, 4 mM KH_2PO_4, pH 7.4, and subjected to Dounce homogenization as we previously described [2]. Briefly, nuclei and debris were removed by 10-min centrifugation at 650 g, and a pellet containing mitochondria (HM) was obtained by 2 successive spins at 10,000 g for 12 min. To obtain the S100 cytosolic fraction and the microsomal pellet, the post mitochondria supernatant was further centrifuged at 100,000 g for 1 h at 4°C.

Secretion assay

CTSD secretion was detected as previously described [71]. The tested cells were incubated in serum-free DMEM

containing cycloheximide (100 μg/ml) at 37°C for the indicated time points. Medium samples were collected, concentrated by 10% TCA at 4°C overnight. Precipitated proteins were pelleted at 16,000 x g for 10 min at 4°C, washed in ice-cold acetone twice, air-dried, resuspended in SDS sample buffer, separated by SDS-PAGE, and immunoblotted. Equal loading was determined by immunoblotting of the cell lysates.

Enzyme activity assays

GUSB (glucuronidase beta) enzymatic activity was tested with a BioVision fluorometric assay kit (K514) according to the manufacturer's protocol. In principle, the assay uses a specific substrate that is cleaved by GUSB into a fluorescent product. The GLB1 (galactosidase beta) activity was determined with a Thermo Scientific fluorometric assay kit (75,707).

Statistical analysis

All immunoblot analyses are representative of at least three experiments. Images are representative of approximately 50 cells from at least three repeats. Quantification by Metamorph was performed on at least 50 cells per treatment, and the results were confirmed in 3 independent experiments. Error bars represent means ± SEM. Statistical analysis was performed by GraphPad Prism 8 software, utilizing either the parametric Student's t-test or the nonparametric Mann-Whitney *U* (MWU) test, as appropriate. Statistical significance is denoted as follows: *** = $p < 0.0001$; ** = $p < 0.001$; * = $p < 0.05$.

Acknowledgments

We thank Richard Flavell (Yale University) and Tak W. Mak, (University Health Network, Toronto, Ontario, Canada) for providing the *casp9* knockout MEF cell lines, and Terje Johansen (University of Tromso, Tromso, Norway) for *EGFP-Rab7a* plasmid.

Disclosure statement

The authors have no conflict of interest with the content of this article.

Funding

This work was supported in part, by the Merit Review Award I01 BX002307 and the Department of Defense Grants W81XWH-15-1-0048, W81XWH-16-1-0213, and W81XWH-20-1-0005 (to H.R.). In addition, this project used the UPCI Cell and Tissue Imaging Facility and the Genomics Research Core that are supported in part by award P30CA047904.

References

[1] Han J, Hou W, Goldstein LA, et al. A complex between Atg7 and Caspase-9: A novel mechanism of cross-regulation between autophagy and apoptosis. J Biol Chem. 2014;289:6485–6497.
[2] Han J, Goldstein LA, Hou W, et al. HSP90 inhibition targets autophagy and induces a caspase-9-dependent resistance mechanism in NSCLC. Autophagy. 2018;1–14. DOI:10.1080/15548627.2018.1434471
[3] An HK, Chung KM, Park H, et al. CASP9 (caspase 9) is essential for autophagosome maturation through regulation of mitochondrial homeostasis. Autophagy. 2019. 1–20. DOI:10.1080/15548627.2019.1695398
[4] Yi CH, Yuan J. The Jekyll and Hyde functions of caspases. Dev Cell. 2009;16:21–34.
[5] Henry CM, Martin SJ. Caspase-8 Acts in a non-enzymatic role as a Scaffold for assembly of a pro-inflammatory "FADDosome" complex upon TRAIL stimulation. Mol Cell. 2017;65(715–29):e5.
[6] Murray TV, McMahon JM, Howley BA, et al. A non-apoptotic role for caspase-9 in muscle differentiation. J Cell Sci. 2008;121:3786–3793.
[7] Jeong HS, Choi HY, Lee ER, et al. Involvement of caspase-9 in autophagy-mediated cell survival pathway. Biochim Biophys Acta. 2010;1813:80–90.
[8] Klumperman J, Raposo G. The complex ultrastructure of the endolysosomal system. Cold Spring Harb Perspect Biol. 2014;6:a016857.
[9] Luzio JP, Hackmann Y, Dieckmann NM, et al. The biogenesis of lysosomes and lysosome-related organelles. Cold Spring Harb Perspect Biol. 2014;6:a016840.
[10] Klionsky DJ, Eskelinen EL, Deretic V. Autophagosomes, phagosomes, autolysosomes, phagolysosomes, autophagolysosomes … wait, I'm confused. Autophagy. 2014;10:549–551.
[11] Eskelinen EL. Maturation of autophagic vacuoles in mammalian cells. Autophagy. 2005;1:1–10.
[12] Coutinho MF, Prata MJ, Alves S. Mannose-6-phosphate pathway: a review on its role in lysosomal function and dysfunction. Mol Genet Metab. 2012;105:542–550.
[13] Braulke T, Bonifacino JS. Sorting of lysosomal proteins. Biochim Biophys Acta. 2009;1793:605–614.
[14] Burd C, Cullen PJ. Retromer: a master conductor of endosome sorting. Cold Spring Harb Perspect Biol. 2014;6:a016774–a016774.
[15] Seaman MN. The retromer complex - endosomal protein recycling and beyond. J Cell Sci. 2012;125:4693–4702.
[16] Gallon M, Cullen PJ. Retromer and sorting nexins in endosomal sorting. Biochem Soc Trans. 2015;43:33–47.
[17] Priya A, Kalaidzidis IV, Kalaidzidis Y, et al. Molecular insights into Rab7-mediated endosomal recruitment of core retromer: deciphering the role of Vps26 and Vps35. Traffic. 2015;16:68–84.
[18] Lucas M, Gershlick DC, Vidaurrazaga A, et al. Structural mechanism for cargo recognition by the retromer complex. Cell. 2016;167:1623–35 e14.
[19] Stein MP, Cao C, Tessema M, et al. Interaction and functional analyses of human VPS34/p150 phosphatidylinositol 3-kinase complex with Rab7. Methods Enzymol. 2005;403:628–649.
[20] McGough IJ, Cullen PJ. Recent advances in retromer biology. Traffic. 2011;12:963–971.
[21] Popoff V, Mardones GA, Bai SK, et al. Analysis of articulation between clathrin and retromer in retrograde sorting on early endosomes. Traffic. 2009;10:1868–1880.
[22] Shi A, Sun L, Banerjee R, et al. Regulation of endosomal clathrin and retromer-mediated endosome to Golgi retrograde transport by the J-domain protein RME-8. Embo J. 2009;28:3290–3302.
[23] Wenzel EM, Schultz SW, Schink KO, et al. Concerted ESCRT and clathrin recruitment waves define the timing and morphology of intraluminal vesicle formation. Nat Commun. 2018;9:2932.
[24] Raiborg C, Wesche J, Malerod L, et al. Flat clathrin coats on endosomes mediate degradative protein sorting by scaffolding Hrs in dynamic microdomains. J Cell Sci. 2006;119:2414–2424.
[25] Kvainickas A, Jimenez-Orgaz A, Nagele H, et al. Cargo-selective SNX-BAR proteins mediate retromer trimer independent retrograde transport. J Cell Biol. 2017;216:3677–3693.
[26] Simonetti B, Paul B, Chaudhari K, et al. Molecular identification of a BAR domain-containing coat complex for endosomal recycling of transmembrane proteins. Nat Cell Biol. 2019;21:1219–1233.
[27] Seaman MN. Cargo-selective endosomal sorting for retrieval to the Golgi requires retromer. J Cell Biol. 2004;165:111–122.
[28] Arighi CN, Hartnell LM, Aguilar RC, et al. Role of the mammalian retromer in sorting of the cation-independent mannose 6-phosphate receptor. J Cell Biol. 2004;165:123–133.
[29] Miura E, Hasegawa T, Konno M, et al. VPS35 dysfunction impairs lysosomal degradation of alpha-synuclein and exacerbates

neurotoxicity in a drosophila model of Parkinson's disease. Neurobiol Dis. 2014;71:1–13.
[30] Wassmer T, Attar N, Bujny MV, et al. A loss-of-function screen reveals SNX5 and SNX6 as potential components of the mammalian retromer. J Cell Sci. 2007;120:45–54.
[31] McGough IJ, Steinberg F, Jia D, et al. Retromer **bindi**ng to FAM21 and the WASH complex is perturbed by the Parkinson disease-linked VPS35(D620N) mutation. Curr Biol. 2014;24:1678.
[32] Osborne DG, Phillips-Krawczak CA, Billadeau DD. Monitoring receptor trafficking following retromer and WASH deregulation. Methods Cell Biol. 2015;130:199–213.
[33] Seaman MNJ. Retromer and the cation-independent mannose 6-phosphate receptor-time for a trial separation? Traffic. 2018;19:150–152.
[34] Simonetti B, Danson CM, Heesom KJ, et al. Sequence-dependent cargo recognition by SNX-BARs mediates retromer-independent transport of CI-MPR. J Cell Biol. 2017;216:3695–3712.
[35] Cui Y, Carosi JM, Yang Z, et al. Retromer has a selective function in cargo sorting via endosome transport carriers. J Cell Biol. 2019;218:615–31.
[36] Kuida K, Haydar TF, Kuan CY, et al. Reduced apoptosis and cytochrome c-mediated caspase activation in mice lacking caspase 9. Cell. 1998;94:325–337.
[37] Hakem R, Hakem A, Duncan GS, et al. Differential requirement for caspase 9 in apoptotic pathways in vivo. Cell. 1998;94:339–352.
[38] Fan T, Huang Z, Wang W, et al. Proteasome inhibition promotes autophagy and protects from endoplasmic reticulum stress in rat alveolar macrophages exposed to hypoxia-reoxygenation injury. J Cell Physiol. 2018;233:6748–6758.
[39] Demishtein A, Fraiberg M, Berko D, et al. SQSTM1/p62-mediated autophagy compensates for loss of proteasome polyubiquitin recruiting capacity. Autophagy. 2017;13:1697–1708.
[40] Kocaturk NM, Gozuacik D. Crosstalk between mammalian autophagy and the ubiquitin-proteasome system. Front Cell Dev Biol. 2018;6:128.
[41] Korolchuk VI, Menzies FM, Rubinsztein DC. Mechanisms of cross-talk between the ubiquitin-proteasome and autophagy-lysosome systems. FEBS Lett. 2010;584:1393–1398.
[42] van Waarde-verhagen M, Kampinga HH. Measurement of chaperone-mediated effects on polyglutamine protein aggregation by the filter trap assay. Methods Mol Biol. 2018;1709:59–74.
[43] Eenjes E, Yang-Klingler YJ, Yamamoto A. Monitoring aggregate clearance and formation in cell-based assays. Methods Mol Biol. 2019;1873:157–169.
[44] Saridaki T, Nippold M, Dinter E, et al. FYCO1 mediates clearance of alpha-synuclein aggregates through a Rab7-dependent mechanism. J Neurochem. 2018;146:474–492.
[45] Chandra D, Tang DG. Mitochondrially localized active caspase-9 and caspase-3 result mostly from translocation from the cytosol and partly from caspase-mediated activation in the organelle. Lack of evidence for Apaf-1-mediated procaspase-9 activation in the mitochondria. J Biol Chem. 2003;278:17408–17420.
[46] Ludwig T, Munier-Lehmann H, Bauer U, et al. Differential sorting of lysosomal enzymes in mannose 6-phosphate receptor-deficient fibroblasts. Embo J. 1994;13:3430–3437.
[47] Ludwig T, Ovitt CE, Bauer U, et al. Targeted disruption of the mouse cation-dependent mannose 6-phosphate receptor results in partial missorting of multiple lysosomal enzymes. Embo J. 1993;12:5225–5235.
[48] Sohar I, Sleat D, Gong Liu C, et al. Mouse mutants lacking the cation-independent mannose 6-phosphate/insulin-like growth factor II receptor are impaired in lysosomal enzyme transport: comparison of cation-independent and cation-dependent mannose 6-phosphate receptor-deficient mice. Biochem J. 1998;330 (Pt 2):903–908.
[49] Munier-Lehmann H, Mauxion F, Bauer U, et al. Re-expression of the mannose 6-phosphate receptors in receptor-deficient fibroblasts. Complementary function of the two mannose 6-phosphate receptors in lysosomal enzyme targeting. J Biol Chem. 1996;271:15166–15174.
[50] Progida C, Cogli L, Piro F, et al. Rab7b controls trafficking from endosomes to the TGN. J Cell Sci. 2010;123:1480–1491.
[51] Hao YH, Doyle JM, Ramanathan S, et al. Regulation of WASH-dependent actin polymerization and protein trafficking by ubiquitination. Cell. 2013;152:1051–1064.
[52] Girard M, Poupon V, Blondeau F, et al. The DnaJ-domain protein RME-8 functions in endosomal trafficking. J Biol Chem. 2005;280:40135–40143.
[53] Chen CS, Chen WN, Zhou M, et al. Probing the cathepsin D using a BODIPY FL-pepstatin A: applications in fluorescence polarization and microscopy. J Biochem Biophys Methods. 2000;42:137–151.
[54] Cullen PJ, Steinberg F. To degrade or not to degrade: mechanisms and significance of endocytic recycling. Nat Rev Mol Cell Biol. 2018;19:679–696.
[55] Frankel EB, Audhya A. ESCRT-dependent cargo sorting at multivesicular endosomes. Semin Cell Dev Biol. 2018;74:4–10.
[56] Bright NA, Davis LJ, Luzio JP. Endolysosomes are the principal intracellular sites of acid hydrolase activity. Curr Biol. 2016;26:2233–2245.
[57] Raiborg C, Bache KG, Mehlum A, et al. Hrs recruits clathrin to early endosomes. Embo J. 2001;20:5008–5021.
[58] Checinska A, Giaccone G, Rodriguez JA, et al. Comparative proteomics analysis of caspase-9-protein complexes in untreated and cytochrome c/dATP stimulated lysates of NSCLC cells. J Proteomics. 2009;1793:605–614.
[59] Sonnichsen B, De Renzis S, Nielsen E, et al. Distinct membrane domains on endosomes in the recycling pathway visualized by multicolor imaging of Rab4, Rab5, and Rab11. J Cell Biol. 2000;149:901–914.
[60] Bache KG, Raiborg C, Mehlum A, et al. Phosphorylation of Hrs downstream of the epidermal growth factor receptor. Eur J Biochem. 2002;269:3881–3887.
[61] Norris A, Tammineni P, Wang S, et al. SNX-1 and RME-8 oppose the assembly of HGRS-1/ESCRT-0 degradative microdomains on endosomes. Proc Natl Acad Sci U S A. 2017;114:E307–E16.
[62] van Weering JR, Sessions RB, Traer CJ, et al. Molecular basis for SNX-BAR-mediated assembly of distinct endosomal sorting tubules. Embo J. 2012;31:4466–4480.
[63] Carlton J, Bujny M, Peter BJ, et al. Sorting nexin-1 mediates tubular endosome-to-TGN transport through coincidence sensing of high- curvature membranes and 3-phosphoinositides. Curr Biol. 2004;14:1791–1800.
[64] Hong Z, Yang Y, Zhang C, et al. The retromer component SNX6 interacts with dynactin p150(Glued) and mediates endosome-to-TGN transport. Cell Res. 2009;19:1334–1349.
[65] Pankiv S, Alemu EA, Brech A, et al. FYCO1 is a Rab7 effector that binds to LC3 and PI3P to mediate microtubule plus end-directed vesicle transport. J Cell Biol. 2010;188:253–269.
[66] Han J, Goldstein LA, Hou W, et al. Deregulation of mitochondrial membrane potential by mitochondrial insertion of granzyme B and direct Hax-1 cleavage. J Biol Chem. 2010;285: 22461–22472.
[67] Han J, Goldstein LA, Hou W, et al. Functional linkage between NOXA and bim in mitochondrial apoptotic events. J Biol Chem. 2007;282:16223–16231.
[68] Han J, Goldstein LA, Hou W, et al. Regulation of mitochondrial apoptotic events by p53-mediated disruption of complexes between antiapoptotic Bcl-2 members and bim. J Biol Chem. 2010;285:22473–22483.
[69] Han J, Hou W, Goldstein LA, et al. Involvement of protective autophagy in TRAIL resistance of apoptosis-defective tumor cells. J Biol Chem. 2008;283:19665–19677.
[70] Dupont N, Leroy C, Hamai A, et al. Long-lived protein degradation during autophagy. Methods Enzymol. 2017;588:31–40.
[71] Rojas R, van Vlijmen T, Mardones GA, et al. Regulation of retromer recruitment to endosomes by sequential action of Rab5 and Rab7. J Cell Biol. 2008;183:513–526.